

3D Numerical Simulation of Flow and Local Scour around a Spur Dike

Guodong Li

Professor, State Key Laboratory of Eco-Hydraulic Engineering in Shaanxi, Xi'an University of Technology, Xi'an 710048, China. Email: gdli2008@xaut.edu.cn

Lan Lang

Graduate student, College of Water Resources and Hydroelectric Engineering, Xi'an University of Technology, Xi'an 710048, China. Email: mitian@xaut.edu.cn

Jian Ning

Graduate student, College of Water Resources and Hydroelectric Engineering, Xi'an University of Technology, Xi'an 710048, China. Email: ningjian@xaut.edu.cn

ABSTRACT: The present paper uses FLOW-3D software to simulate the three-dimensional flow and local scour around a non-submerged spur dike. The Navier-Stokes equations are solved with Finite Volume Method. Selected turbulence model is RNG κ - ϵ model and the bed-load transport model is based on Shields number. The volume of fluid (VOF) method is employed in FLOW-3D tracking fluid-air or fluid-fluid interfaces. Simulated results of mean flow and turbulence for fixed bed case include backflow length, the distribution of velocity, turbulent energy and dissipation. This provides a theoretical foundation for explaining erosion mechanism. For movable bed, the results verify that all of the scour process can be divided into three stages: initial stage, main scour stages and balance stage, most of the scour is completed in the first two stages. Obtained depth and scope of scoured pit around spur dike coincide well with experiment. The analysis of flow field distribution shows that the formation of the scoured surface is mainly influenced by submerged flow and horseshoe vortex. In main scour stage, the intensity of submerged flow and horseshoe vortex increased rapidly, so the scour pit depth increased accordingly. With the increasing of the depth of scour pit, the flow velocity decreases, submerged flow and horseshoe vortex strength decreased until water flow velocity reduced to cannot take away the sediment.

KEY WORDS: Spur dike, Local scour, Numerical simulation

1 INTRODUCTION

Spur dike is a kind of hydraulic structure that is widely used to redirect flows, protect river bank, adjust water depth and build local deposition. The construction of the spur dike can locally change the river flow pattern, and at the same time, the complex backflow and vortexes will be formed in the tail of the dike. Accordingly, scour and silting existing around spur dikes have great significance on stability and security of the structure. Therefore studying the flow and predicting volume of local scour in the vicinity of dike will have important engineering significance.

In addition to some of theoretical analysis, there are many experiment investigations and field observations have been conducted on scour mechanism, influencing factors, flow structure, scour depth and backflow length, etc. since 1930. With the rapid development of the computer, numerical simulation has become an effective research means. For instance Tingsanchali and Maheswaran (1990) calculated the distribution of bed shear stress near the dike by two-dimensional average depth model and improved $k - \epsilon$ turbulence model; Michiue and Hinokidai (1992) completed the two-dimensional calculation of erosion and deposition near the dike, the results are in good agreement with those of experimental observation; Zhongwei Li and Minghui Yu (2000) used the flow function equation and vorticity equation to simulate local flow fields around the normal spur dike with various discharges and various dike lengths. Compared the simulating results of the flow fields with the indoor experimental results, the both agree

well with each other.

In general, some achievements have been made in spur dikes, but most of the existing researches are based on model test, and less work has been done on the numerical simulation. Furthermore, much less research work has been done on the influence of the turbulence flow field, bed shear stress, and sediment transport on the scour depth. In addition, the parameters affecting the scour depth have not been fully understood. This paper use FLOW-3D software to simulate the three-dimensional flow and local scour around a non-submerged spur dike. The related flow fields are analyzed, in order to further deepen the understanding of the scour mechanism.

2 NUMERICAL MODEL AND METHOD

2.1 Numerical Model

2.1.1 Governing equations

The governing equations of flow are the continuity equation and the momentum equation:

$$\frac{\partial u_i}{\partial x_i} = 0, \quad (1)$$

$$\frac{\partial u_i}{\partial t} + u_j \frac{\partial u_i}{\partial x_j} = -\frac{1}{\rho} \frac{\partial P}{\partial x_i} + \frac{\partial}{\partial x_j} (2\nu S_{ij} - \overline{u'_i u'_j}), \quad (2)$$

where

$$S_{ij} = \frac{1}{2} \left(\frac{\partial u_i}{\partial x_j} + \frac{\partial u_j}{\partial x_i} \right), \quad (3)$$

$$\overline{u'_i u'_j} = \nu_t \left(\frac{\partial u_i}{\partial x_j} + \frac{\partial u_j}{\partial x_i} \right) - \frac{2}{3} k \delta_{ij}. \quad (4)$$

where u_i is the fluid velocity component in i direction, u'_i is the fluctuation of fluid velocity in i direction, P is the pressure, S_{ij} is the mean strain rate tensor, $\overline{u'_i u'_j}$ is the Reynolds stress tensor, ρ is the fluid density, ν is the fluid kinetic viscosity, ν_t is the turbulence viscosity, k is the turbulent kinetic energy, and δ_{ij} is the Kronecker delta ($\delta_{ij} = 1, i = j; \delta_{ij} = 0, i \neq j$).

2.1.2 Turbulence model

Yakhot and Orszag (1986) proposed an improved $k - \varepsilon$ turbulence model that is named RNG (renormalization group) $k - \varepsilon$ model, in which the coefficients are not obtained from experimental data, but the theoretical analysis. The RNG $k - \varepsilon$ model has better adaptability than standard $k - \varepsilon$ model. This study uses RNG $k - \varepsilon$ model to simulate the spur dike turbulent flow, combines with the standard wall function method to deal with the near wall. The governing equations are as follows:

$$\frac{\partial k}{\partial t} + u_j \frac{\partial k}{\partial x_j} = \tau_{ij} \frac{\partial u_i}{\partial x_j} + \frac{\partial}{\partial x_j} \left[\frac{1}{\rho} \left(\mu + \frac{\mu_t}{\sigma_k} \right) \frac{\partial k}{\partial x_j} \right] - \varepsilon \quad (5)$$

$$\frac{\partial \varepsilon}{\partial t} + u_j \frac{\partial \varepsilon}{\partial x_j} = C_{1\varepsilon} \frac{\varepsilon}{k} \tau_{ij} \frac{\partial u_i}{\partial x_j} + \frac{\partial}{\partial x_j} \left[\frac{1}{\rho} \left(\mu + \frac{\mu_t}{\sigma_k} \right) \frac{\partial \varepsilon}{\partial x_j} \right] - C_{2\varepsilon} \rho \frac{\varepsilon^2}{k} \quad (6)$$

where k is the turbulent kinetic energy, $k = \frac{1}{2} \overline{u'_i u'_i}$; ε is the dissipation of turbulent kinetic energy,

$\varepsilon = \nu \left(\frac{\partial u'_i}{\partial x_k} \right) \left(\frac{\partial u'_i}{\partial x_k} \right)$; μ_t is the turbulent eddy viscosity, $\mu_t = c_\mu \rho k^2 / \varepsilon$; τ_{ij} is the Reynolds stress,

$\tau_{ij} = \frac{\mu_t}{\rho} \left(\frac{\partial u_i}{\partial x_j} + \frac{\partial u_j}{\partial x_i} \right) - \frac{2}{3} \rho k \delta_{ij}$; the constants are $c_\mu = 0.085$, $C_{1\varepsilon} = 1.42$, $C_{2\varepsilon} = 1.68$, $\sigma_k = 0.7179$, $\sigma_\varepsilon = 0.7179$.

2.1.3 Sediment transport model

The bed-load model used in this study is similar to the model described by Chen (2006) that ignores the influence of the suspend sediment, only the bed-load sediment is considered and the sediments are uniform. At present, there are five primary methods available for studying the transport rule of bed-load sediment, they are flow velocity, drag force, energy balance, statistical law and sand wave movement(Zhang,1998). This paper employs the bed-load sediment transport rate formula dependent on drag force to study the bed-load sediment. This type of formula takes the drag force as the main factor in calculating the bed-load sediment transport rate. The sediment transport rate increases with the drag force.

The definitions of flow drag force τ 、critical drag force of sediment incipient motion τ_c 、Shields number θ and critical Shields number θ_c are as follows:

$$\tau = \rho U_*^2, \quad (7)$$

$$\tau_c = \rho U_{*c}^2, \quad (8)$$

$$\theta = \frac{\tau}{g(\rho_s - \rho)d}, \quad (9)$$

$$\theta_c = \frac{\tau_c}{g(\rho_s - \rho)d}. \quad (10)$$

where U_* is the friction velocity, U_{*c} is the critical friction velocity, ρ is the flow density, ρ_s is the sand density, d is the mean sediment diameter.

Engelund and Fredsoe (1976)supposed the formula of bed-load transport rate in1976 as follows:

$$q_b = \rho_s \frac{\pi}{6} d^3 \frac{1}{d^2} u_b p, \quad (11)$$

where q_b is the bed-load transport rate in unit width. u_b is the mean transport velocity of bed-load, and p is the motion probability of bed surface sediment particles. As shown in eq. (11), the bed-load transport rate is determined only by u_b and p for particular sediment.

The driving force on a single particle is

$$F_D = C_D \frac{\pi}{4} d^2 \rho \frac{(aU_* - u_b)^2}{2} \quad (12)$$

The friction force is

$$f_D = g(\rho_s - \rho) \frac{\pi}{6} d^3 \beta \quad (13)$$

The driving force F_D is equal to the friction force f_D thus

$$\frac{u_b}{U_*} = a \left(1 - \sqrt{\frac{4\beta}{3a^2 C_D \theta}} \right) \quad (14)$$

Letting $\theta_0 = \frac{4\beta}{3a^2 C_D}$, there will be

$$\frac{u_b}{U_*} = a \left(1 - \sqrt{\frac{\theta_0}{\theta}} \right) \quad (15)$$

where C_D is the coefficient of the driving force, and aU_* is the water velocity where bed-load sand is moving. In the zone near the bed $a=6-10$. When $\theta = \theta_0$, $u_b = 0$, in other words, θ_0 is equivalent to the

relative drag force that prevents sediment from moving; therefore, θ_0 is less than the critical relative drag force θ_c . Eq. (16) is then obtained by rewriting eq. (15):

$$\frac{u_b}{U_*} = a \left(1 - 0.7 \sqrt{\frac{\theta_0}{\theta}} \right) \quad (16)$$

The drag force is the sum of the critical drag force acting on the sandy bed and the drag force acting on the moving sediment particles, which is described as follows:

$$\tau = \tau_c + n g (\rho_s - \rho) \frac{\pi}{6} d^3 \beta \quad (17)$$

where n is the quantity of sediment particles. The relationship between the quantity of sand particles in the unit bed area $\frac{1}{d^2}$ and the probability for sand moving p is $p = n / \frac{1}{d^2}$. Considering eqs. (9) and (10), we can get the following expression for p :

$$p = \frac{6}{\pi \beta} (\theta - \theta_c) \quad (18)$$

As mentioned above, u_b and p are the two determined factors of the bed-load transport rate q_b . By substituting the u_b and p obtained from eq. (16) and eq. (18) into eq. (11) respectively, the formula describing the bed-load sediment transport rate is deduced as follows with the dynamic friction coefficient $\beta = 0.8$ and the constant $a = 9.3$:

$$q_b = \begin{cases} 11.6 \rho_s d (\theta - \theta_c) (\sqrt{\theta} - 0.7 \sqrt{\theta_c}), & \theta \geq \theta_c \\ 0, & \theta < \theta_c \end{cases} \quad (19)$$

which is the bed-load model used in this paper. Eqs. (16), (18) and (19) show that for certain sediments, the bed-load model is primarily determined by Shields number. The scour occurs in beds where the Shields number reaches the critical Shields number. In this paper, the critical Shields number is $\theta_c = 0.033$.

2.2 Grid System and Numerical Methods

For the sake of comparison, the computational domain in the study is the same to experimental apparatus of Zhang Hao(2009). The flume is 4m-long, 0.4m-wide, 0.25m-deep and the slope is 1/1000, the roughness factor is 0.009. A spur dike is attached to the flume, 1cm-thick and perpendicular to the right side of flume with a protruding length of 10cm. The upstream inlet is placed at a distance of 2m from the spur dike to ensure that the flow becomes fully developed. The water depth is 5cm, the spur dike is non-submerged, and the top of which is about 3cm over the water surface. When calculation is made in moving bed condition covered with 0.15m-thick model sediment, the sediment particles has a mean size of $d = 0.145$ cm and a specific gravity of $s = 1.9$ g/cm. Owing to the complexity of the flow field around the spur dike, the structured non-uniform grid and mesh refinement are employed in the paper. The numbers of the grid is about 600,000 and grid division is shown in Figure 2.

In the paper, finite volume method is used to discrete controlling equations and select RNG $k - \varepsilon$ turbulent model. Water inlet adopts the velocity inlet and the given velocity is 0.29m/s, the water depth is 0.05m. Setting the outlet as an outflow and all of solid walls boundary are considered to be no-slip processed by standard wall function. The VOF method is used to capture the free surface.

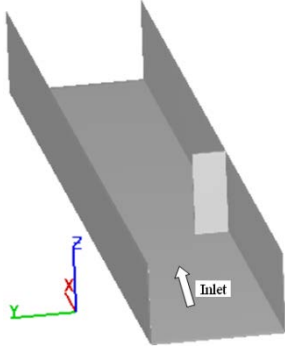


Figure 1 Computational domain

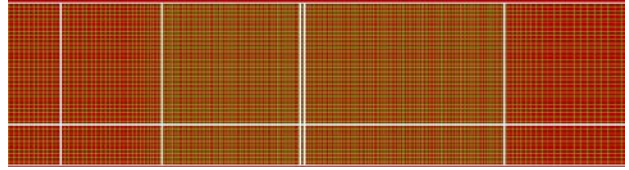


Figure 2 Grid in the vicinity of the spur dike

3 RESULTS AND ANALYSIS

3.1 The Flow Field

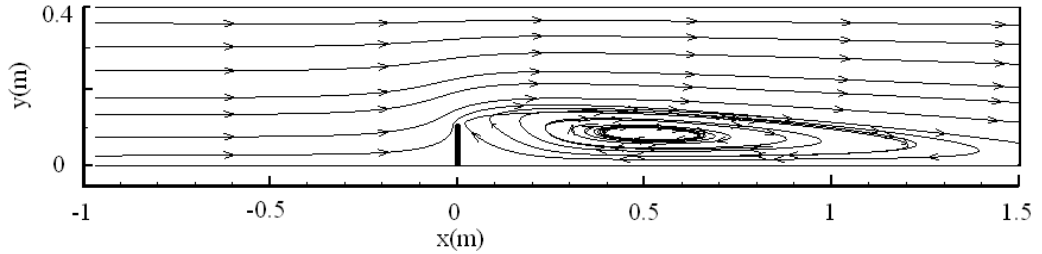


Figure 3 Streamlines

The streamlines around the spur dike is shown in Figure 3. It can be seen that a great clockwise eddy is produced in the wake zone behind the spur dike, whose eddy shape is close to irregular oval, and center is located in the position $x=0.5\text{m}$. In order to analyze the flow velocity distribution in detail, the total velocity and velocity component at the middle section are discussed individually.

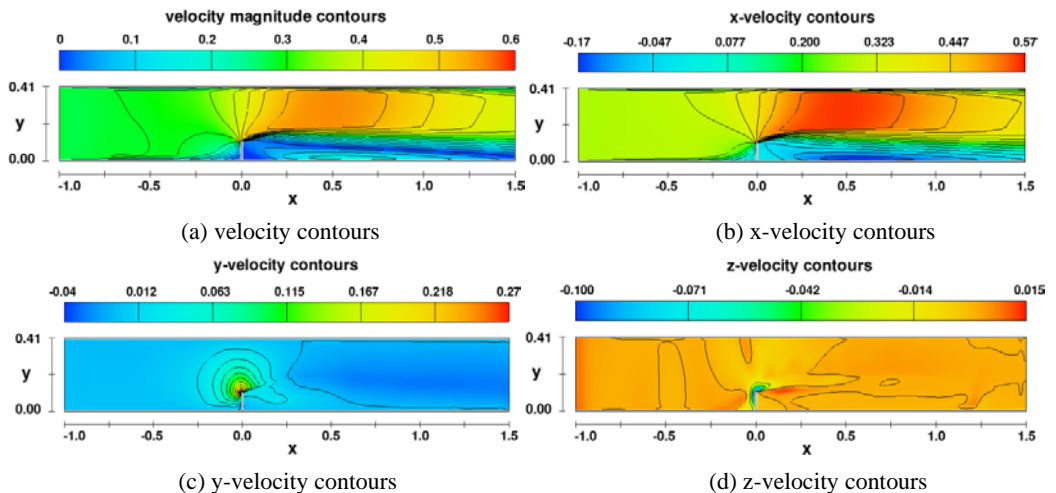


Figure 4 Velocity distributions around the spur dike at middle section

Owing to the presence of spur dike, the velocity is increase rapidly with the decrease of channel wide, the maximum velocity is 0.56m/s. At downstream of the spur dike, the velocity recovers gradually. The water flow goes towards the side of the flume and forms a wake zone with low speed behind the dike where x-velocity appears to have the negative value. In Figure 4 (b), x-velocity component distribution is similar to total velocity's, whose value is near to zero at the end of the spur dike, whereby illustrating that the stagnant zone is produced here. In Figure 4 (c), y-velocity component is so small at the whole field, but sharply amplifies at the tip of the spur dike, and the maximum value is 0.25m/s. There is little difference between the z-velocity and y-velocity in most places, except that shown in Figure 4 (d) where the maximum value is negative at the tip of the spur dike, so that water flows along with the negative direction of z axis, that is the submerged flow.

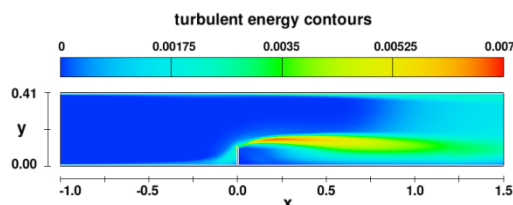


Figure 5 Contours of turbulent energy

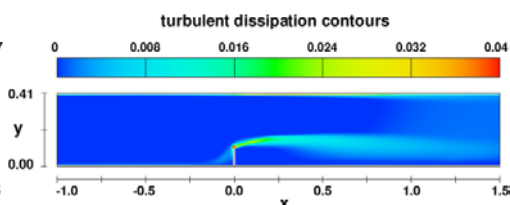


Figure 6 Contours of turbulent dissipation

Turbulent kinetic energy is the representation of the fluid turbulence extent, the more turbulent kinetic energy of fluid, the more tempestuous turbulent and turbulent intensity are. Contours of turbulent at middle section $z=0.025\text{m}$ are shown in Figure 5. The turbulent kinetic energy is very small in most area where value of fluctuating velocity is small, so that the turbulent kinetic energy $k = \frac{1}{2}(u'^2 + v'^2 + w'^2)$ is diminutive too. In the border of mainstream and the wake zone where turbulent intensity is so large that the maximum value of the turbulent kinetic energy appears in this position.

Turbulent dissipation is a kind of conversion rate among various kinds of energy. It is representative of a rate that is mechanical energy converted into heat energy with isotropic small scale eddy in turbulent flow. The larger the dissipation rate is, and so is the energy loss. Contours of turbulent dissipation at middle section $z=0.025\text{m}$ is shown in Fig.6 whose distribution is very close to the turbulent energy distribution. The maximum value take place in the tip of the dike, where the flow shear is most serious.

3.2 Scour Analysis

Scour development around spur dike in different times is shown in Figures 7-8. The result displays that scour equilibrium condition is reach after 80min. At this moment, scour pit is deepest in the tip of the spur dike, and the scour in upstream side is more serious than downstream side, so that the scour pit in upstream is deeper and the slope is steeper. Meanwhile, different shapes of the sand wave is generated at the whole bed, being consistent with the experiment result(Jing ect. 2002). In Figure 8 (d), the maximum scour depth at the equilibrium condition is 7.8cm in upstream with the slope of 35° on the verge of angle of repose and the length of 19cm. Compared with upstream, the scour slope in downstream is a half of it, the scour depth is 6.5cm, but the length of the scour pit is far outweigh the upstream, being about 32 cm. According to experimental measurements, the maximum scour hole depth is 11.5cm (70% of the equilibrium depth), but length is close to experiment. As to the development speed of the scour pit, three stages can obviously observed: initial stage, main scour stage and balance stage. Local scour develops rapidly in the first several minutes and showed insignificant changes after balance stage, most of the scour is completed in the first two stages, and this can prove Peng Jing conclusion.

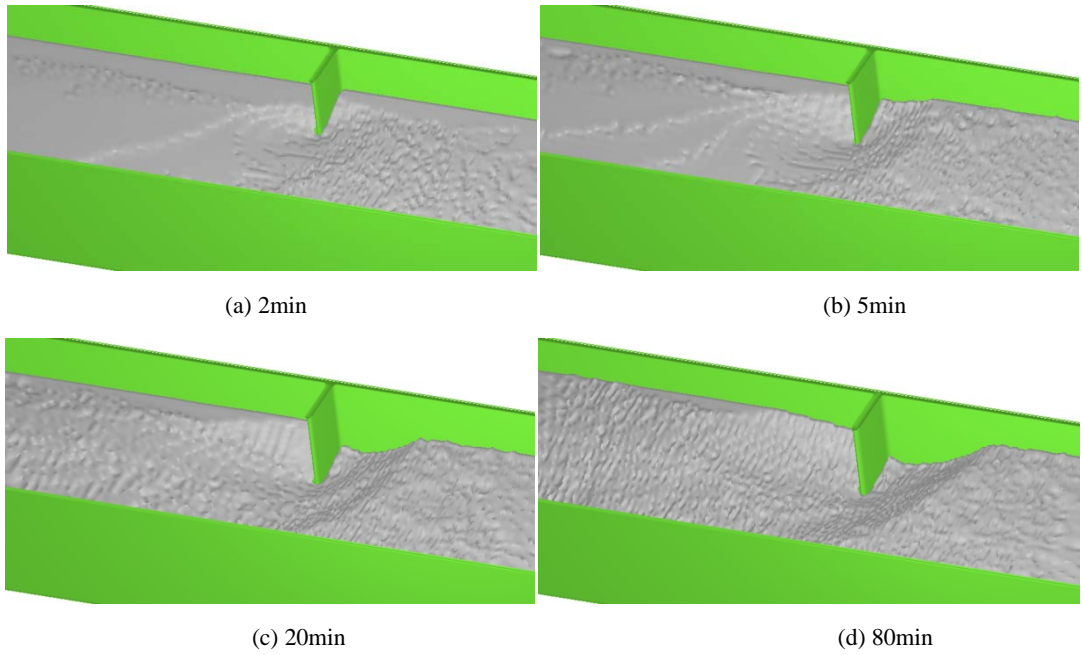


Figure 7 Scour development around spur dike in different times

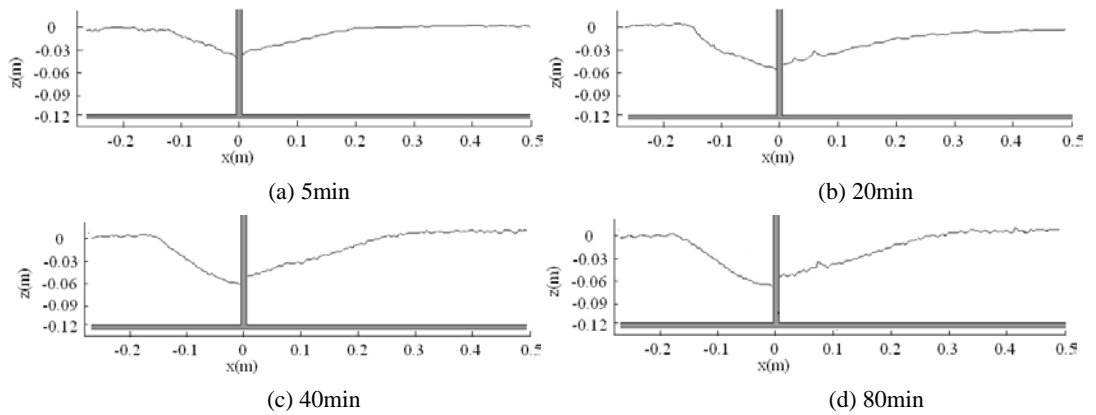


Figure 8 Scour development at section $y=0.1\text{m}$ in different times

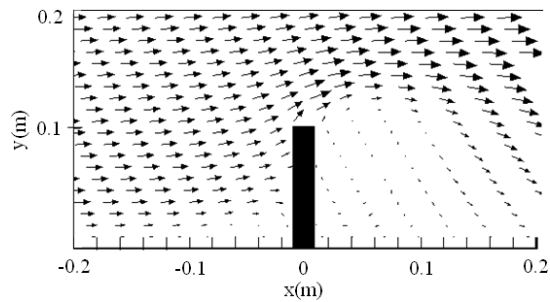


Figure 9 Velocity vectors at the water surface

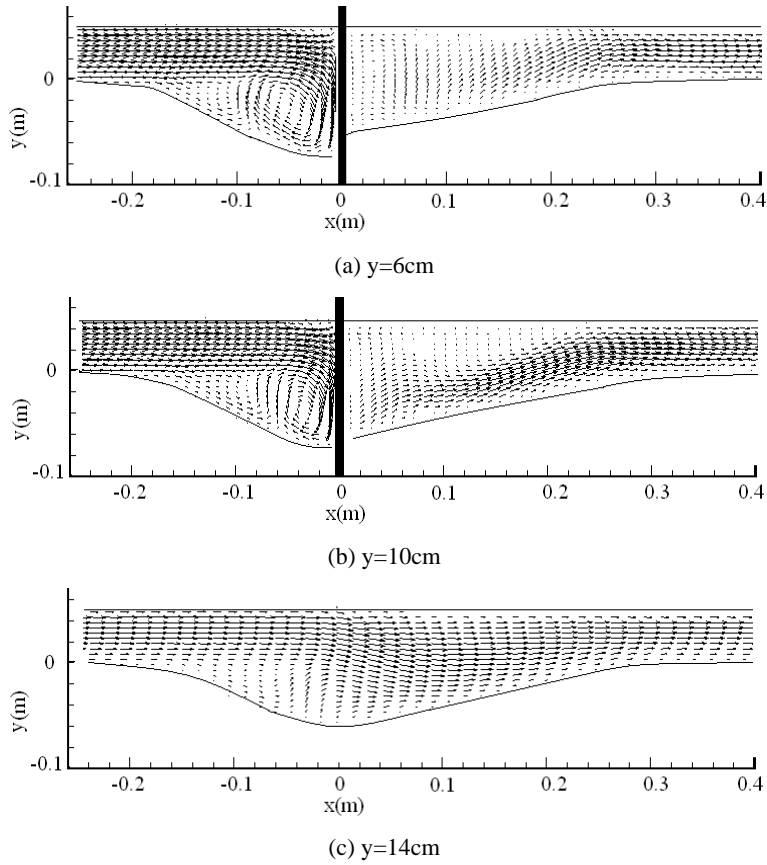


Figure 10 Velocity vectors at longitudinal section

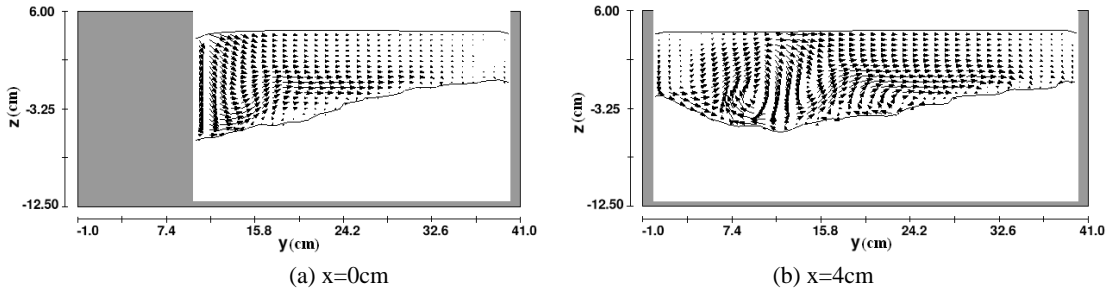


Figure 11 Velocity vectors at transverse section

The velocity vectors (u, v) on the water surface in the neighborhood of the spur dyke are shown in Figure 9. It can be seen that the flow approaches the spur dyke, it can be diverted into three parts on the surface. One part is to accelerate and separate the main channel. This flow separation is believed to play an important role on scour process. The other part goes towards the side of the flume and forms an anti-clockwise eddy at the corner. In addition, the stream forms the diving flow in front of the spur dike as the result of downward dynamic water pressure gradient caused by velocity difference. The advanced flow turns into the scour pit and forms an anti-clockwise horseshoe vortex flow which is main vortex formed by rotation. The diving flow and horseshoe vortex in front of spur dike can be observed evidently in Figure 10 (a) and (b). In main scour stage, the intensity of submerged flow and horseshoe vortex increased so rapidly, that the scour pit depth increased. With the augment in the depth of scour pit, the flow velocity decreases submerged flow and horseshoe vortex strength decrease until water flow velocity

so reduced that it cannot take away the sediment. By this time, the depth of scour pit is maximized. Moreover, there are two rotating cells in Figure 11(b), in addition to the horseshoe vortex at the head of the spur dike, there is another vortex system in the wake zone area. This vortex is in an opposite direction compared with the horse-shoe vortex and independent from the horse-shoe vortex and occupies most of the water column, in which vortex has certain effect on the development of the scour pit.

4 CONCLUSIONS

(1) Numerical simulation results show that mathematical models and numerical methods used in the study can better simulate the dynamic procedure of the scour around spur dike. The scour pit development with the time was observed dividing three stages obviously: initial stage, main scour stage and balance stage, and the most scour is completed in the first two stages.

(2) Based on analysis of the flow in fix bed and move-bed, the formation of the obtained scour is mainly influenced by submerged flow and horseshoe vortex. In main scour stage, the enhancement of intensity of submerged flow and horseshoe vortex make the scour pit depth increasing rapidly. With the augment in the depth of scour pit, the flow velocity decreases, submerged flow and horseshoe vortex strength decrease until water flow velocity is so reduced that it cannot take away the sediments.

(3) Owing to the complexity of turbulent flow and sediment movement around the spur dike, scour pit depth and scope is not very ideal to compare with the experimental value. Except for sediment scour model, there is a certain relationship with parameter calibration and this need to be further improve in the future study.

References

- Chen B. The numerical simulation of local scour in front of a vertical-wall breakwater[J]. *Journal of Hydrodynamics*, Ser. B. 2006, 18(3): 134-138.
- Duan, J. G. Mean flow and turbulence around an experimental spur dike. *J. Hydraul. Eng.*, 2009, 134 (3), 315-327.
- Engelund F, Fredsoe J. A sediment transport model for straight alluvial channels [J]. *Nordic Hydrology*. 1976, 7(5): 293-306.
- LI Zhong-we, YU Ming-hui. Numerical simulation of local flow field around spur dike. *Wuhan university journal of hydraulic and electric engineering*, 2000, 33(3): 18-22.
- Michiue, M., and Hinokidani, O., Calculation of 2dimensional Bed Evolution around S pur-dike , *Annual Journal of Hydraulic Engineering , JSCE , 1992, Vol . 36: 61 - 66.*
- Pan Qing-shen, Yu Wen-chou et al., Research summary of spur dike in foreign [J]. *Yangtze River*, 1979, (3):51-61.
- Peng Jing, Nobuyuki Tamai, Y oshihisa K awahara. Numerical modeling of local scour around spur dikes. *Journal of Sediment Research*. 2002(1):25-29.
- Tingsanchali T, Maheswaran S. 2-D depth-averaged flow computation near groyne. *Journal of Hydraulic Engineering*, ASCE, 1990, 116(1): 71-86.
- Yakhot V, Orszag S A. Renormalization-group analysis of turbulence [J]. *Physical review letters*. 1986, 57(14): 1722-1724.
- Ying Qiang, Jiao Zhi-bin. *Hydraulic Properties of Groyne* [M]. Beijing: Maritime Press, 2004.
- Zhang Hao, Hajime NAKAGAWA et al. Experiment and simulation of turbulent flow in local scour around a spur dyke. *International Journal of Sediment Research*, Vol. 24, No. 1, 2009:33-45.
- Zhang Rui-jin. *River sediment dynamics*. [M]. Beijing: China Water Power Press, 1998.
- Zhang, H., Nakagawa, H., Ishigaki, T, and Muto, Y. Prediction of 3D flow field and local scouring around spur dikes. *Ann. J. Hydraul. Eng.*, 2005, 49, 1003–1008.